Charge Photogeneration and Transport in AgBiS$_2$ Nanocrystal Films for Photovoltaics

Diedenhofen, Silke L.; Bernechea, Maria; Felter, Kevin M.; Grozema, Ferdinand C.; Siebbeles, Laurens D.A.

Important note
To cite this publication, please use the final published version (if applicable).
Please check the document version above.

Charge Photogeneration and Transport in AgBiS$_2$ Nanocrystal Films for Photovoltaics

Silke L. Diedenhofen, Maria Bernechea,* Kevin M. Felter, Ferdinand C. Grozema, and Laurens D. A. Siebbeles*

Solution-processed AgBiS$_2$ nanocrystal films are a promising material for non-toxic, earth-abundant solar cells. While solar cells with good device efficiency are demonstrated, so far, hardly anything is known about charge generation, transport, and recombination processes in these films. Here, a photoinduced time-resolved microwave conductivity study on AgBiS$_2$ nanocrystal films is presented. By modeling the experimental data with density-dependent recombination processes, the product of the temperature-dependent electron and hole quantum yield and mobility, and the electron and hole recombination kinetics are determined.

1. Introduction

Solution-processed nanocrystals are good candidates to solve the demand for low-cost and easily processable solar cell materials.[1] To date, the most efficient nanocrystal solar cells are based on toxic lead chalcogenides.[2,3] Therefore, there is a strive for non-toxic, earth-abundant solar cell materials. A very promising solar cell material consists of AgBiS$_2$ nanocrystals.[4–6] Recently, a solar cell based on AgBiS$_2$ nanocrystals has been demonstrated with a certified power conversion efficiency of 6.3%, for an active film thickness of only 35 nm.[4] So far, very little is known about the photogeneration, charge transport, and charge recombination dynamics in AgBiS$_2$ nanocrystal films. These properties depend on the size of the nanocrystals and on their local environment, such as the type of ligands. Pejova et al.[7,8] studied the photoconductivity and relaxation dynamics in sonochemically synthesized assemblies of AgBiS$_2$ quantum dots. The authors found that under low light intensity, trap-assisted (Shockley–Read–Hall) recombination is the dominant electron–hole decay mechanism with an average hole lifetime of 1.67 ms. Hu et al. aimed to improve the solar cell device efficiency via an amine-based synthesis route.[5] The nanocrystals used for this solar cell are smaller than the ones used by Bernechea et al.,[4] with a diameter of 2.8 nm. They found a mobility of 4.1×10^{-5} cm^2 V^{-1} s^{-1} in a field-effect transistor geometry. To obtain a better understanding of the properties of AgBiS$_2$, density functional theory (DFT) calculations have been carried out and from which the Bohr exciton radius ($r_B = 4.6$ nm) has been obtained, as well as the effective masses of electrons ($m_e = 0.35\, m_0$) and holes ($m_h = 0.722\, m_0$), with m$_0$ the free electron mass.[9] In addition, the influence of cationic disorder on the electronic structure of AgBiS$_2$ has been studied, and it has been found that the temperature triggers cationic disorder resulting in a reduced bandgap, a substantial reduction of the conduction band edge with a slight increase of the valence band. The authors state that this might lead to less efficient exciton recombination, which has a beneficial effect on the photoconductivity of AgBiS$_2$ samples.[10]

While solution-processed AgBiS$_2$ solar cells have been fabricated with very promising power conversion efficiencies, hardly anything is known with regard to the recombination dynamics and electrical transport in AgBiS$_2$ nanocrystal thin films. Therefore, we present here a study of the photogeneration, mobility, and recombination kinetics of free charges in films of AgBiS$_2$ nanocrystals. We utilize photoinduced time-resolved microwave conductivity (TRMC) experiments[11] to determine the temperature-dependent charge carrier quantum yield, carrier mobilities, and lifetimes. The sample is photoexcited with a short laser pulse with a controlled photon fluence, and we measure the change in photoconductance as a change in absorbed microwave power upon photoexcitation as a function of time, see Experimental Section. By modeling the experimental data with recombination mechanisms, we can determine the decay times and the product of charge carrier quantum yield and mobility.

Dr. S. L. Diedenhofen, K. M. Felter, Dr. F. C. Grozema,
Prof. L. D. A. Siebbeles
Faculty of Applied Sciences
Delft University of Technology
Van der Maasweg 9, 2629 HZ Delft, The Netherlands
E-mail: s.l.diedenhofen@tudelft.nl

Dr. M. Bernechea
ARAID
Government of Aragon
50018 Zaragoza, Spain
E-mail: mbernechea@unizar.es

Dr. M. Bernechea
Institute of Nanoscience of Aragon (INA)
University of Zaragoza
50018 Zaragoza, Spain

Dr. M. Bernechea
Cardiff School of Engineering
Cardiff University
Cardiff CF24 3AA, Wales, UK

2. Results and Discussion

AgBiS$_2$ nanocrystals have been synthesized following the recipe described by Bernechea et al.,[4] and AgBiS$_2$ nanocrystal films were prepared following a layer-by-layer (LBL) deposition procedure on fused silica substrates using tetramethylammonium iodide (TMAI) as the capping ligands. We have chosen TMAI as a capping ligand as AgBiS$_2$ solar cells with this ligand showed best performance.[4] In PbS colloidal quantum dot films, it has been shown that the halide capping ligands result in energetically shallower electron trap states compared with the case of the best organic ligand treatments.[12] Halide-capped colloidal quantum dot films have a lower density of trapped carriers, due in part to the lower trap density and in part to electron and hole recombination. Halide-capped PbS colloidal quantum dot solids have on average a smaller trap state energy measured relative to the conduction band. The lower average trap energy from the halide treatment also results in higher average mobility. To conclude, halide ligand passivation enables good passivation of surface defects, high carrier mobility, and good device stability as compared with organic ligands.[12]

It has been demonstrated that the performance of PbS quantum dot solar cells can be increased by a molecular iodine treatment applied before the solid-state ligand exchange. This iodine treatment results in a twofold decrease in trap density and, therefore, improves the charge carrier diffusion length in PbS quantum dot films.[13] To investigate if we can improve the charge carrier mobility and/or the lifetime in AgBiS$_2$ nanocrystal films, we prepared films using iodine-treated AgBiS$_2$ nanocrystals analogously to the iodine treatment of PbS quantum dots. From X-ray photoelectron spectroscopy (XPS), we found that the iodine treatment resulted in an iodine incorporation of 2% I:Bi ratio (see Supporting Information). Thereafter, an untreated AgBiS$_2$ nanocrystal film refers to the film prepared using as-synthesized AgBiS$_2$ nanocrystals and TMAI as capping ligands. The thickness of the samples is determined to be 50 ± 5 nm by Dektak profiling.

To characterize the optical quality of the AgBiS$_2$ films, we measured the absorption coefficient of the untreated and iodine-treated AgBiS$_2$ nanocrystal films (**Figure 1**). Both films have an absorption coefficient on the order of 10^5 cm^{-1} for wavelengths shorter than 750 nm with the untreated film absorbing slightly stronger. Both films do not show a clear absorption onset at the electronic bandgap ($\approx$1.3 eV, $\approx$950 nm)[14] of AgBiS$_2$ nanocrystals. We attribute this absorption tail below the bandgap to absorption due to excitation of electrons to/from trap states in the bandgap. Photographs of the untreated and iodine-treated AgBiS$_2$ nanocrystal films show that the films are very dark and brownish, demonstrating the strong absorbance in films with a thickness of only 50 ± 5 nm (inset in Figure 1). For a solar cell, an optimum thickness of 35 nm has been found,[4] which is due to an optimal combination of charge carrier extraction efficiency and optical interference in the film; in our case, the thickness is less crucial. First, this is because our sample is an AgBiS$_2$ nanocrystal film on fused silica with different conditions for optical interference than in a solar cell configuration. Second, charges are not extracted in TRMC experiments but charge transport is measured within the nanocrystal film, so that the charges do not have to travel across the thickness of the film. To confirm that the AgBiS$_2$ nanocrystals used in this study are the same as
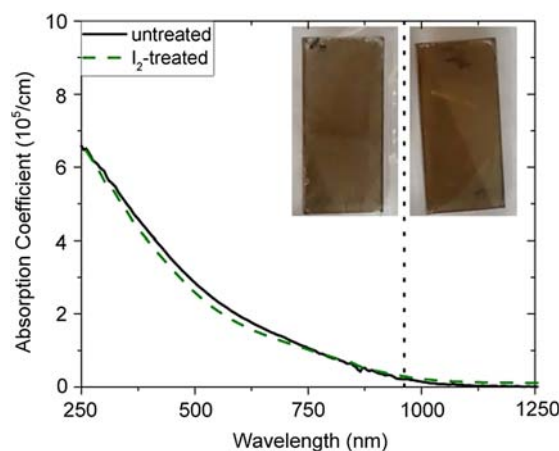

Figure 1. Absorption coefficient of a standard AgBiS$_2$ nanocrystal film (black solid curve) and of an iodine-treated AgBiS$_2$ nanocrystal film (green dashed curve). The energy bandgap at 1.3 eV is marked with the dotted line. The inset shows the photographs of the untreated (left) and I$_2$-treated (right) films.

the ones used for the best performing solar cell,[4] we performed transmission electron microscopy on the nanocrystals. The untreated AgBiS$_2$ nanocrystals have a diameter of 5 ± 3 nm and the I$_2$-treated nanocrystals of 7 ± 3 nm. Therefore, we can conclude that the untreated AgBiS$_2$ nanocrystals are the same as the nanocrystals used by Bernechea et al.[4] The TEM images and size histograms are provided in the Supporting Information.

We utilized the TRMC technique to determine the temperature-dependent photogeneration yield, mobility, and decay dynamics of charge carriers. We illuminated the film with 3 ns laser pulses with a wavelength of 420 nm, and we determined the photoconductance as a function of time. In TRMC, the photoconductance normalized to the incident photon fluence (I_0) is given by

$$S(t) = \frac{\Delta G}{\beta e I_0} = \left(\mu_\mathrm{n} \frac{n(t)}{I_0} + \mu_\mathrm{p} \frac{p(t)}{I_0} \right) d \tag{1}$$

where ΔG is the photoconductance, β is the ratio of the inner dimensions of the microwave cell, e is the electron charge, I_0 is the incident photon fluence, d is the thickness of the film, μ_n and μ_p are the mobility of electrons and holes, respectively, and $n(t)$ and $p(t)$ are the photoexcited electron and hole concentration, respectively. At the end of the pulse and before the charge carriers recombine, the normalized photoconductance is proportional to the photogenerated charge carrier yield $\phi_0 = n(t = 0)I_0^{-1} = p(t = 0)I_0^{-1}$ and the sum of the mobilities of electrons and holes. The incident photon fluence is determined from optical energy measurements. More details are given in the Experimental Section.

Figure 2a shows normalized photoconductance transients for an untreated AgBiS$_2$ film at 298 and 173 K. The normalized photoconductances show an initial increase with time due to free carrier generation during the 3 ns laser pulse and reach a maximum as a result of the balance of charge generation and decay. The normalized photoconductance at 298 K subsequently decays due to charge recombination or trapping. The maximum photoconductance is significantly reduced with decreasing temperature, indicating either a lower charge carrier mobility or a
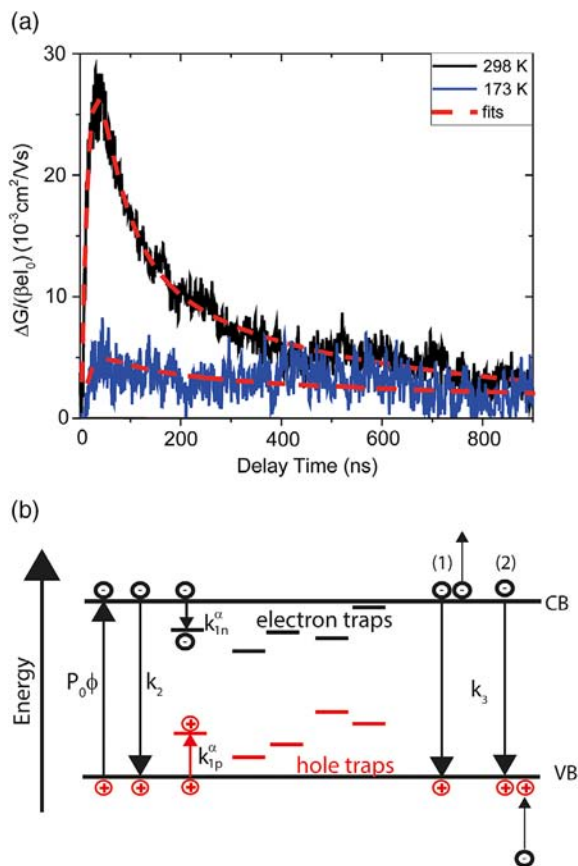
Figure 2. a) Experimental normalized photoconductance of the untreated AgBiS$_2$ nanocrystal film measured at 298 K (black solid curve) and 173 K (blue solid curve) and fits to the measurements (dashed curves). b) Energy diagram showing the recombination mechanisms used to describe the time-dependent microwave conductivity data. P_o is the number of absorbed photons per unit volume and unit time and ϕ_0 is the quantum yield of charge carriers. $k^{\alpha}_{1p,n}$ are stretch parameters due to the distribution of trap states for electrons (black) and holes (red) below the conduction band (CB) and above the valence band (VB). k_2 is the radiative recombination rate constant and k_3 is the Auger recombination rate constant.

lower photogenerated charge carrier yield. While the normalized photoconductance at 298 K decays with an initial fast component, the normalized photoconductance at 173 K decays much slower and is less significant in the 1 µs time range in Figure 2a. At delay times longer than 500 ns, both normalized photoconductances decay similarly. For normalized photoconductances smaller than 10×10^{-3} cm^2 V^{-1} s^{-1}, the measurement is influenced by random noise in the microwave detection setup. The noise may be caused by wiring, microwave sensor, or other electrical components. However, the signal-to-noise ratio is sufficient to neglect these effects in our data treatment. To get quantitative information about the photogenerated quantum yield, mobility, and decay kinetics, we employ the model schematically shown in Figure 2b: free charges are generated upon photoexcitation by a photon pulse P_0 (number of absorbed photons per unit volume and unit time) and a quantum yield ϕ. These free charges can get trapped or recombine via different routes. As absorption

measurements revealed the absence of a clear absorption onset at the electronic bandgap, it can be inferred that the trap states exist. Therefore, we include electron and hole trapping in the model. In a disordered system, electron or hole trap states can exist that are located at different energies in the bandgap. This distribution of energies results in a stretched exponential decay rate according to $n(t) = n(t = 0)e^{-(k_{1n}t)^{\alpha}}$.[15] The same holds for an energetic distribution of hole trap states at energies above the valence band, with rate constant k_{1p}. $n(t)$ and $p(t)$ are the time-dependent concentrations of free electrons and holes, respectively. The other two recombination pathways are the second-order radiative recombination, with decay rate constant k_2, and the third-order Auger recombination, with decay rate constant k_3.[16] For simplicity, we assume that the Auger recombination rate is the same if an electron from the conduction band recombines with a hole in the valence band and excites thereby an electron from the conduction band to a higher band (case 1), or if the recombination of an electron from the conduction band with a hole from the valence band excites an electron from a lower band recombining with a hole in the valence band (case 2). This model results in differential Equation (2) and (3) for electrons and holes. The stretch parameter α in these equations depends on the temperature as $\alpha = T/T_0$,[15] with T_0 being the energetic width of the distribution of trap states.

$$\frac{dn(t)}{dt} = P_0\phi - \alpha k_{1n}(tk_{1n})^{\alpha-1}n(t) - k_2 n(t)p(t)$$
$$- k_3(n^2(t)p(t) + n(t)p^2(t)) \tag{2}$$

$$\frac{dp(t)}{dt} = P_0\phi - \alpha k_{1p}(tk_{1p})^{\alpha-1}p(t) - k_2 n(t)p(t)$$
$$- k_3(n^2(t)p(t) + n(t)p^2(t)) \tag{3}$$

To fit our experimental data, we employ Equation (1) with $n(t)$ and $p(t)$ from Equation (2) and (3). From theoretical work where the effective mass of an electron (m_n) and a hole (m_p) was determined, we take $\frac{\mu_p}{\mu_n} = \frac{m_n}{m_p} = \frac{1}{2.06}$, where μ_p is the mobility of holes and μ_n is the mobility of electrons,[9] assuming that the scattering times for electrons and holes are equal. This model was fit to our measurements. Details about the fitting routine and the dependence of the fit on the individual parameters are given in the Experimental Section and the Supporting Information.

In Figure 2a, the measured data are shown together with fits of Equation (1)–(3), demonstrating an excellent agreement between measurement and fit. While performing these measurements, we made sure that the normalized photoconductance is independent of the incident photon fluence by choosing sufficiently low photon fluences. In this case, only the first-order recombination or trapping processes are leading to decay of the signal. Therefore, in these fits, the higher order recombination processes (rate constants k_2 and k_3) could be neglected, and the fitting parameters are ϕ, k_{1n}, k_{1p}, T_0, and μ_n. From the fits, we find an energetic width of the trap states of $E_t = k_B T_0 = 43 \pm 1$ meV, with k_B being the Boltzmann constant.

To determine the temperature dependence of the charge carrier mobilities and decay rates, we have performed TRMC measurements at temperatures between 298 and 148 K in steps of 25 K, and we have fitted Equation (1)–(3) to the data. The results
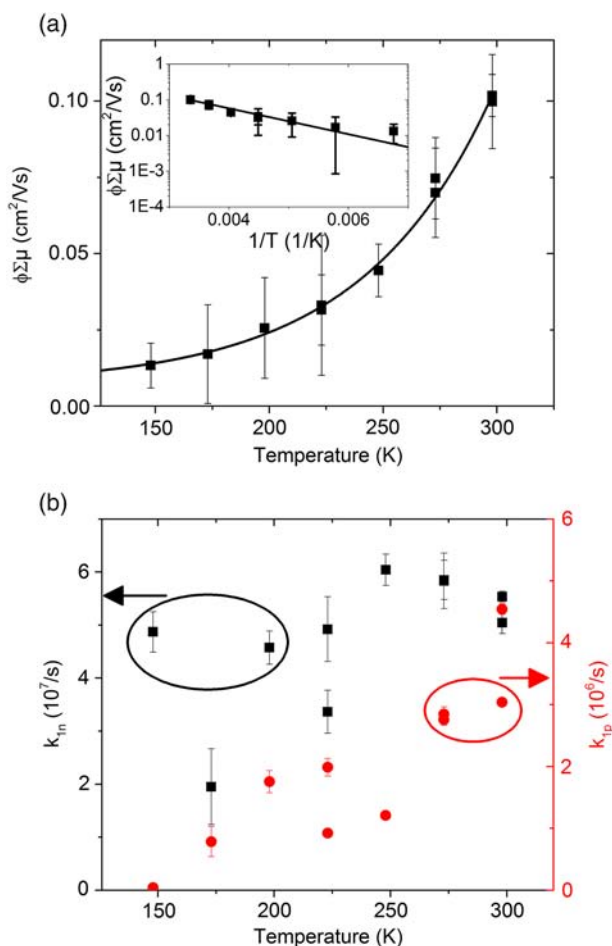
Figure 3. Temperature-dependent a) product of charge carrier generation yield and sum of electron and hole mobilities and b) first-order decay rates of electrons (black squares) and holes (red circles) of the untreated AgBiS$_2$ nanocrystal film. The curve in (a) is an exponential fit to the measurement and serves as a guide to the eye. The inset in (a) shows the same data as in the main figure, plotted as an Arrhenius plot. The solid line is a linear fit to the experimental data.

of these fits are displayed in **Figure 3**. To make sure that sample heating during optical excitation does not influence our data, we have determined the maximum temperature change upon excitation. For the photon fluence used in this experiment, the maximum temperature change is ≈20 mK, which is not significant. More details about this calculation are given in the Supporting Information. At 248, 273, and 298 K, two measurements are performed, one after decreasing the temperature and the other after increasing the temperature. The difference of the obtained values for the measurements taken at the same

wavelengths is a good indication of the experimental error. The charge carrier generation yield and the charge carrier mobilities cannot be fit independently. Therefore, the product of the charge carrier generation yield and the sum of electron and hole mobilities ($\phi\Sigma\mu = \phi(\mu_n + \mu_p)$) are shown in Figure 3a. $\phi\Sigma\mu$ increases exponentially with temperature from $(13 \pm 7) \times 10^{-3}$ cm^2 V^{-1} s^{-1} at 148 K to $(100 \pm 15) \times 10^{-3}$ cm^2 V^{-1} s^{-1} at 298 K. $\phi\Sigma\mu$ found in AgBiS$_2$ nanocrystals is higher than that found in Bi$_2$S$_3$ nanocrystals, which is on the order of 10^{-2} cm^2 V^{-1} s^{-1} at 300 K.[17] This might explain why AgBiS$_2$ outperforms Bi$_2$S$_3$ solar cells.[18] However, this value is lower than $\phi\Sigma\mu$ found in PbSe quantum dots, depending on the surface passivation ligand varies from 10^{-2} to 0.8 cm^2 V^{-1} s^{-1} at 300 K.[19] The inset in Figure 3a shows an Arrhenius plot of the experimental data together with a linear fit. We obtain the activation energy from the slope S of this curve to be $E_a = (31 \pm 7)$ meV.

The decay rates k_{1n} and k_{1p} are shown in Figure 3b. The decay rate for electrons is rather independent on temperature with a value of $(5 \pm 2) \times 10^7$ s^{-1}. The decay rate for holes shows a much stronger dependence on temperature, with an increase of about one order of magnitude from $(4 \pm 1) \times 10^5$ s^{-1} at 148 K to $(4 \pm 1) \times 10^6$ s^{-1} at 298 K. This temperature dependence of the decay rate indicates that hole trapping is thermally activated. All the parameters of the untreated AgBiS$_2$ nanocrystal film are summarized for clarity in **Table 1**. If we assume a charge carrier generation yield of unity, we find the lower limit of the electron mobility being 0.07 cm^2 V^{-1} s^{-1}. As the size of the nanocrystals is close to the exciton Bohr radius of AgBiS$_2$, the exciton binding energy is likely high. Therefore, the charge carrier generation yield is likely much lower than unity, which will result in a higher electron mobility. Knowing the mobility and the decay rate of the excited electrons and holes allows us to determine the lower limit of the diffusion length (L_d) in the AgBiS$_2$ nanocrystal film using the Einstein relation

$$D = \mu \frac{k_B T}{e} \tag{4}$$

and

$$L_d = (D\tau)^{\frac{1}{2}} \tag{5}$$

where D is the diffusion coefficient, μ is the mobility of the charges, k_B is the Boltzmann constant, T is the temperature, e is the electron charge, and τ is the inverse of the decay rate. The diffusion length is the average distance that a charge carrier moves before it is trapped or recombines. From the diffusion length, we can estimate the optimum thickness of the active layer of a solar cell based on AgBiS$_2$ nanocrystals. An electron (hole) mobility of 0.07 cm^2 V^{-1} s^{-1} (0.032 cm^2 V^{-1} s^{-1}) and a decay rate of 4.8×10^7 s^{-1} (3.8×10^6 s^{-1}) result at room temperature in lower limits of the diffusion lengths of 60 and 150 nm for

Table 1. Product of charge generation yield and mobility of electrons and holes ($\phi\Sigma\mu$), first-order electron (k_{1n}) and hole (k_{1p}) decay rates, second-order decay rate (k_2), and third-order decay rate (k_3), lower limits of the diffusion length of electrons ($L_{D,n}$) and holes ($L_{D,p}$), energetic width of the trap states (E_t), and activation energy (E_a) of the untreated AgBiS$_2$ film. The temperature-dependent parameters are given at 298 K.

$\phi\Sigma\mu$ [10^{-3} cm^2 V^{-1} s^{-1}]	$k_{1n(p)}$ [10^6 s^{-1}]	k_2 [10^{-10} cm^3 s^{-1}]	k_3 [10^{-28} cm^6 s^{-1}]	$L_{D,n(p)}$ [nm]	E_t [meV]	E_a [meV]
100 ± 15	50 ± 20 (4 ± 1)	2.5 ± 0.5	2.5 ± 0.5	60 (150)	43 ± 1	31 ± 7

electrons and holes, respectively, indicating that a solar cell based on $AgBiS_2$ nanocrystals should be thinner than 60 nm for efficient charge collection. This result is in agreement with the maximum short-circuit current found by Bernechea et al. in a solar cell with an active layer thickness of 35 nm and a drop in short-circuit current for thicker solar cells.[4] In their case, a thickness of 60 nm is not beneficial as absorption is reduced in the solar cell with this thickness due to destructive optical interference. Using a different solar cell geometry, Pai et al.[6] found a higher short-circuit current density than Bernechea et al.[4] with an active layer thickness of 60 nm. Adapting the thicknesses of the hole and electron transport layers such that the $AgBiS_2$ nanocrystal film can have a thickness of 60 nm without destructive interference of light in this film might increase the efficiency of the solar cell. This can be further studied by performing simulations according to Jiménez-Solano et al.[20] Knowing the lower limit of the diffusion constant also allows us to determine the lower limit of the distance scale over which we probed the charge transport (L_{CT}) in the $AgBiS_2$ nanocrystal film: $L_{CT} \cong (6D\tau_{OS})^{\frac{1}{2}}$, with τ_{OS} being the oscillation time that depends on the electric field frequency by $\tau_{OS} = \frac{2\pi}{\omega}$.[21] With a diffusion constant of $1.8\ cm^2\ s^{-1}$ and a frequency of 8.5 GHz, the lower limit of the distance scale over which charge transport is probed is 28 nm, so roughly over 5 to 6 nanocrystals.

Bernechea et al. found that current collection is more efficient at intensities lower than 1 sun than at higher light intensities, and they attribute this to an intensity-dependent recombination process.[4] To understand more about intensity-dependent recombination processes in $AgBiS_2$ nanocrystal films, we also increased the photon fluence in our measurements until higher order recombination occurred. **Figure 4**a shows the normalized photoconductance measured on the untreated $AgBiS_2$ nanocrystal film with photon fluences of 3.6×10^{11}, 8.6×10^{11}, 7.6×10^{12}, and 3.3×10^{13} photons cm^{-2}. The normalized photoconductance transients measured with higher fluence have a lower maximum value because of the normalization to the incident photon fluence. The change in conductance (ΔG), not normalized to the incident photon fluence, increases with photon fluence. This is also obvious from the reduced noise in the transients measured with high fluences. However, more important than the maximum signal of the four measurements are the decay kinetics of the photoconductance. For clarity, the inset in Figure 4 displays the two transients measured at maximum and minimum photon fluence normalized to their maxima. The high fluence transient decays much faster, indicating that higher order recombination processes are playing a role in this experiment. To emphasize the change in decay kinetics, Figure 4b shows the maximum value of the normalized photoconductance measured at different photon fluences. At low photon fluences ($\approx 10^{11}$ photons cm^{-2}), the curve is flat, indicating that only the first-order recombination is important at this fluence. When increasing the photon fluence, the peak value of the normalized photoconductance is strongly decreasing, indicating that the fluence-dependent higher order recombination occurs. Therefore, we fit the higher fluence normalized photoconductance by including the second-order and Auger recombination as additional recombination pathways (see Figure 2b). From these fits, we found decay rates k_2 and k_3 of $(2.5 \pm 0.5) \times 10^{-10}\ cm^3\ s^{-1}$ and $(2.5 \pm 0.5) \times 10^{-28}\ cm^6\ s^{-1}$,
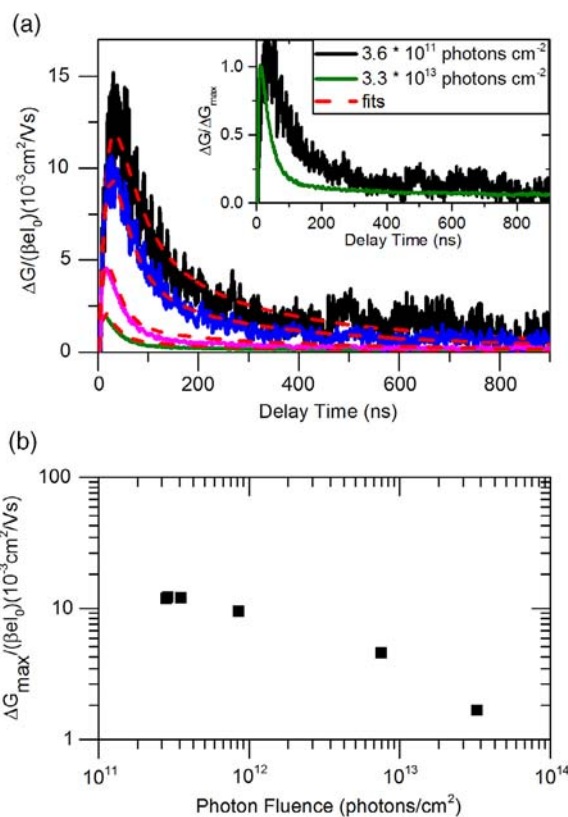

Figure 4. a) Normalized photoconductance (solid curves) and fits (dashed curves) of the untreated $AgBiS_2$ nanocrystal film measured with photon fluences of 3.6×10^{11} (black), 8.6×10^{11} (blue), 7.6×10^{12} (magenta), and 3.3×10^{13} photons cm^{-2} (olive). The inset shows the transients measured at maximum and minimum photon fluences normalized to their maxima. b) The peak value of the normalized photoconductance as a function of photon fluence.

respectively. For solar cells working at 1 sun, these two decay pathways are playing no role, as the light intensity at 1 sun is much lower than the intensities we use in this study. The intensity-dependent recombination of charge carriers found by Bernechea et al. in their solar cells cannot be explained by these recombination processes, as these are occurring at much higher fluences than 1 sun.[4] Therefore, we can conclude that the recombination processes found by Bernechea et al. are related to the solar cell configuration and are not an intrinsic property of $AgBiS_2$ nanocrystal films.

To check if the iodine treatment can decrease the trap density in $AgBiS_2$ nanocrystal films and improve their optoelectronic performance, we measured the photoconductance of the untreated and I_2-treated $AgBiS_2$ films. **Figure 5** shows the photoconductance normalized to the absorbed photon fluence, which is the incident photon fluence times the fraction of absorbed light (F_A) measured on both films at three different photon fluences. The normalized photoconductances measured with similar photon fluence are overlapping. For clarity, the inset in Figure 5 displays the four transients measured at maximum and minimum photon fluences normalized to their maxima. The high fluence measurements of the untreated and the I_2-treated films are
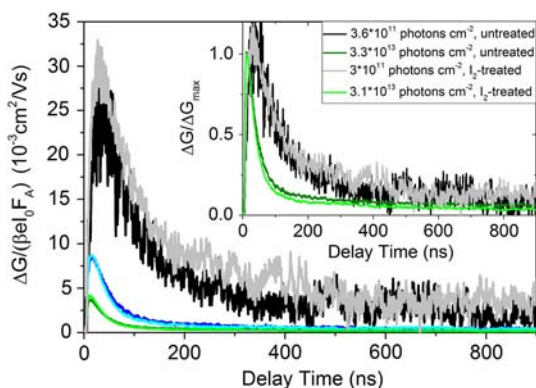
Figure 5. Photoconductance normalized to the absorbed photon fluence (I_0F_A) of the untreated AgBiS$_2$ nanocrystal film measured with photon fluences of 3.6×10^{11} (black), 7.6×10^{12} (blue), and 3.3×10^{13} photons cm^{-2} (olive) and of a iodine-treated AgBiS$_2$ nanocrystal film measured with photon fluences of 3×10^{11} (gray), 8×10^{12} (cyan), and 3.1×10^{13} photons cm^{-2} (green). The inset shows the transients measured at maximum and minimum photon fluences normalized to their maxima.

overlapping as well as the low fluence measurements, indicating that the same fluence-dependent recombination mechanisms occur in both films. Therefore, we conclude that the iodine treatment has no influence on the performance of the AgBiS$_2$ films.

3. Conclusion

We have shown that the product of the charge generation yield and the mobility of electrons and holes in AgBiS$_2$ nanocrystal films is on the order of 10^{-1} cm^2 V^{-1} s^{-1} at room temperature and that at low photon fluences ($\approx 10^{11}$ photons cm^2) electrons and holes decay via trapping at defects. At high photon fluences ($\approx 10^{12}$ photons cm^2), radiative and Auger recombination are also occurring. From the mobility of electrons and the trapping rate, we have determined an electron diffusion length of 60 nm and a hole diffusion length of 150 nm. This study gives hints on how to improve the efficiency of AgBiS$_2$ nanocrystal solar cells, namely, by reducing trap states and optimizing the device thickness for efficient light absorption and carrier extraction. This could be implemented by changes in the synthesis, more efficient passivation schemes, or nanostructuring the active layer.

4. Experimental Section

AgBiS$_2$ Nanocrystal Synthesis: For the synthesis of AgBiS$_2$ nanocrystals, 1 mmol Bi(OAc)$_3$, 0.8 mmol Ag(OAc), and 17 mmol oleic acid (OA) were pumped overnight at 100 °C to form the Bi and Ag oleates and remove oxygen and moisture. The reaction atmosphere was then switched to Ar, and 1 mmol hexamethyldisilathiane (HMS) dissolved in 5 mL 1-octadecene (ODE) was quickly injected into the flask, the heating was stopped (without removing the heating mantel), and the reaction was allowed to cool slowly. Nanocrystals were precipitated after the addition of acetone and centrifugation, purified by successive dispersion in toluene and precipitation with acetone, and finally dispersed in anhydrous toluene. The reaction flasks were protected from light until precipitation of nanocrystals.

I$_2$ Treatment of AgBiS$_2$ Nanocrystals: The process was adapted from ref. [13]. In brief, 0.3 mL of I$_2$ solution in toluene (18×10^{-3} M) was added drop by drop to a vial with 1 mL of a colloidal solution of AgBiS$_2$ (110 mg mL^{-1}). The mixture was kept overnight protected from light. Methanol was added to precipitate the nanocrystals that were cleaned by successive dissolution/precipitation in toluene/methanol. Finally, the nanocrystals were dissolved in anhydrous toluene.

Preparation of AgBiS$_2$ Films: Fused silica (ESCO) substrates ($20 \times 1.5 \times 1$ mm) were cleaned by sonication for 10 min in soapy water, acetone, and finally isopropanol. The 50 nm AgBiS$_2$ nanocrystal film was fabricated, following five rounds of a LBL deposition process using a 20 mg mL^{-1} colloidal solution of AgBiS$_2$ in toluene. The 50 nm thickness was chosen to have an adequate film for spectroscopic studies and to be close to the optimum thickness observed for solar cells. One LBL cycle involved dropping one drop of the AgBiS$_2$ colloidal solution onto the quartz substrate spinning at 1900 rpm and waiting for 10 s, and adding five drops of TMAI (1 mg mL^{-1} in methanol) and waiting for another 20 s; this step was repeated once more. Afterward, the films were rinsed with methanol and toluene. Once the process was repeated five times, the films were annealed in air at 100 °C.

Photoinduced TRMC Experiments: Thin AgBiS$_2$ films on fused silica substrates were loaded into an air tight microwave resonance cavity inside a N$_2$-filled glovebox. The TRMC technique was used to measure the change in microwave (8–9 GHz) power after pulsed excitation (repetition rate 10 Hz) at 420 nm.[11] The photoexcitation-induced change in microwave power is related to the change in conductance ΔG by a sensitivity factor $\frac{\Delta P(t)}{P} = -k\Delta G(t)$. The rise of ΔG is limited by the width of the laser pulse (3.5 ns fwhm) and the response time of our microwave system (18 ns). The slow repetition rate of the laser of 10 Hz ensures full relaxation of all photoinduced charges to the ground state before the next laser pulse hits the sample.

Optical Characterization: The absorption coefficient of the AgBiS$_2$ nanocrystal films was determined by measuring the fraction of absorbed light (A) of the films upon placing the films inside the integrating sphere at an angle of incidence of 8° using a PerkinElmer Lambda900 spectrophotometer and by measuring the fraction of transmitted light (T) of the films upon placing the samples in front of the integrating sphere. Using this technique, the absorption coefficient can be determined by $\alpha = -\ln(\frac{T}{A+T})\frac{1}{d}$. The thickness d of the thin films was determined using a Veeco Dektak 8 Stylus Profilometer.

We have solved the differential Equation (2) and (3) with an ordinary differential equation solver (ODE45) in Matlab and included the result in Equation (1) as a part of a fitting routine using a nonlinear regression model (nlinfit). We have obtained the 95% confidence intervals of the fit parameters using nlparci. These confidence values are used as error bars in Figure 3.

Supporting Information

Supporting Information is available from the Wiley Online Library or from the author.

Conflict of Interest

The authors have no conflict of interest.

[1] Z. Yang, J. Z. Fan, A. H. Proppe, F. P. G. De Arquer, D. Rossouw, O. Voznyy, X. Lan, M. Liu, G. Walters, R. Quintero-Bermudez, B. Sun, S. Hoogland, G. A. Botton, S. O. Kelley, E. H. Sargent, *Nat. Commun.* **2017**, *8*, 1.

[2] X. Lan, O. Voznyy, F. P. García De Arquer, M. Liu, J. Xu, A. H. Proppe, G. Walters, F. Fan, H. Tan, M. Liu, Z. Yang, S. Hoogland, E. H. Sargent, *Nano Lett.* **2016**, *16*, 4630.

[3] E. M. Sanehira, A. R. Marshall, J. A. Christians, S. P. Harvey, P. N. Ciesielski, L. M. Wheeler, P. Schulz, L. Y. Lin, M. C. Beard, J. M. Luther, *Sci. Adv.* **2017**, *3*, eaao4204.

[4] M. Bernechea, N. C. Miller, G. Xercavins, D. So, A. Stavrinadis, G. Konstantatos, *Nat. Photonics* **2016**, *10*, 521.

[5] L. Hu, R. Patterson, Z. Zhang, Y. Hu, D. Li, Z. Chen, L. Yuan, G. Conibeer, S. Huang, *J. Mater. Chem. C* **2018**, *6*, 731.

[6] N. Pai, J. Lu, D. C. Senevirathna, A. S. R. Chesman, T. Gengenbach, M. Chatti, U. Bach, P. C. Andrews, L. Spiccia, Y. B. Cheng, A. N. Simonov, *J. Mater. Chem. C* **2018**, *6*, 2483.

[7] B. Pejova, D. Nesheva, Z. Aneva, A. Petrova, *J. Phys. Chem. C* **2011**, *115*, 37.

[8] B. Pejova, I. Grozdanov, D. Nesheva, A. Petrova, *Chem. Mater.* **2008**, *20*, 2551.

[9] F. Viñes, M. Bernechea, G. Konstantatos, F. Illas, *Phys. Rev. B* **2016**, *235203*, 1.

[10] F. Viñes, G. Konstantatos, F. Illas, *Phys. Chem. Chem. Phys.* **2017**, *19*, 27940.

[11] T. J. Savenije, A. J. Ferguson, N. Kopidakis, G. Rumbles, *J. Phys. Chem. C* **2013**, *117*, 24085.

[12] J. Tang, K. W. Kemp, S. Hoogland, K. S. Jeong, H. Liu, L. Levina, M. Furukawa, X. Wang, R. Debnath, D. Cha, K. W. Chou, A. Fischer, A. Amassian, J. B. Asbury, E. H. Sargent, *Nat. Mater.* **2011**, *10*, 765.

[13] X. Lan, O. Voznyy, A. Kiani, F. P. García De Arquer, A. S. Abbas, G. H. Kim, M. Liu, Z. Yang, G. Walters, J. Xu, M. Yuan, Z. Ning, F. Fan, P. Kanjanaboos, I. Kramer, D. Zhitomirsky, P. Lee, A. Perelgut, S. Hoogland, E. H. Sargent, *Adv. Mater.* **2016**, *28*, 299.

[14] P. Huang, W. Yang, M. Lee, *J. Phys. Chem. Cem. C* **2013**, *117*, 18308.

[15] G. Dicker, M. P. De Haas, D. M. De Leeuw, L. D. A. Siebbeles, *Chem. Phys. Lett.* **2005**, *402*, 370.

[16] J. Piprek, *Semiconductor Optoelectronic Devies*, Academic Press, San Diego **2003**.

[17] R. Nishikubo, A. Saeki, *J. Phys. Chem. Lett.* **2018**, *9*, 5392.

[18] N. C. Miller, M. Bernechea, *APL Mater.* **2018**, *6*, 84503.

[19] C. S. S. Sandeep, S. Ten Cate, J. M. Schins, T. J. Savenije, Y. Liu, M. Law, S. Kinge, A. J. Houtepen, L. D. A. Siebbeles, *Nat. Commun.* **2013**, *4*, 1.

[20] A. Jiménez-Solano, J. F. Galisteo-López, H. Míguez, *J. Phys. Chem. Lett.* **2018**, *9*, 2077.

[21] F. C. Grozema, L. D. A. Siebbeles, *J. Phys. Chem. Lett.* **2011**, *2*, 2951.